Performance of Inequality Index Detectors Implemented with Direct-Conversion Receivers

Luiz Gustavo Barros Guedes and Dayan Adionel Guimarães

Abstract— **Inequality index-based detectors represent promising techniques for cooperative spectrum sensing in cognitive radio networks. While schemes such as the Gini index detector (GID), Pietra-Ricci index detector (PRIDe), Atkinson index detector (AID), and Theil index detector (TID) have been studied, prior work typically assumes ideal conditions with conventional receiver models. The impact of impairments from direct-conversion receivers (DCR), including quantization, clipping, and DC-offset, remains underexplored. This work addresses that gap by evaluating these detectors under both conventional and DCR-based models. Results show that PRIDe is the most robust, while TID is particularly sensitive to realistic distortions.**

Keywords— **Cooperative spectrum sensing, cognitive radio, inequality index detectors, direct-conversion receiver.**

I. Introduction

The exponential growth in demand for new wireless communication systems and services, whether in current or future generations of mobile networks, has brought renewed attention to two fundamental limitations in spectrum utilization [1]. First, spectrum scarcity arises from the lack of availability of new frequency bands. Second, spectrum underutilization occurs due to the intermittent activity of primary users (PUs), who hold exclusive rights to use specific bands under traditional fixed spectrum allocation policies. These challenges motivate the development of dynamic spectrum access (DSA) [2] techniques, wherein secondary users (SUs), for example, opportunistically access temporarily unoccupied portions of the spectrum without causing harmful interference to the PUs.

One of the enabling technologies for DSA is spectrum sensing [3], a fundamental capability in cognitive radio networks. In this context, SUs autonomously monitor a particular frequency band to identify potential transmission opportunities. Spectrum sensing is typically formulated as a binary hypothesis testing problem: the null hypothesis, $\mathcal{H}_0$, assumes the absence of PU signal within the sensed frequency band, whereas the alternative hypothesis, $\mathcal{H}_1$, assumes its presence. This sensing approach can be performed individually by a single SU or collectively by a group of SUs through cooperative spectrum sensing (CSS). Owing to its potential to improve detection accuracy in the presence of fading and shadowing, CSS is generally favored over individual sensing strategies.

Luiz Gustavo Barros Guedes and Dayan Adionel Guimarães are with the National Institute of Telecommunications (Inatel), Santa Rita do Sapucaí, MG, Brazil (e-mails: {dayan; luizgustavo.barros}@inatel.br). This work was funded by resources from the following agencies: RNP/MCTI (Grant 01245.010604/2020-14), EMBRAPII/MCTI (Grants 052/2023 PPI IoT/Manufatura 4.0, PPE-00124-23), FAPESP (Grants 22/09319-9, 20/05127-2), FAPEMIG (Grants APQ-04523-23, APQ-05305-23, APQ-01558-24, RED-00194-23), and CNPq (Grant 302589/2021-0).

In a CSS with data fusion, cooperating SUs independently collect signal samples and report them to a central entity known as the fusion center (FC). The FC processes the received data to compute a global test statistic, T, which is then compared against a decision threshold, λ. If $T < \lambda$, then hypothesis $\mathcal{H}_0$ is accepted; otherwise, $\mathcal{H}_0$ is rejected. The performance of spectrum sensing systems is quantitatively characterized by two primary metrics: the probability of detection, P_{d}, which measures the likelihood of correctly detecting an active PU; and the probability of false alarm, P_{fa}, which corresponds to erroneously detecting a PU signal when it is actually absent.

Apart from the effects of wireless channel propagation, noise and interference, performance degradation in spectrum sensing is influenced by the impairments imposed by the architectural design of the receiver [4], [5]. Notably, many models employed in the spectrum sensing literature simplify the receiver structure, often neglecting realistic aspects of signal processing encountered in practical implementations. This motivates the need for performance analysis under more realistic receiver architectures, which can better capture the operational constraints and impairments of actual cognitive radio systems.

Among diverse detection techniques, detectors based on inequality indices have emerged as promising alternatives for spectrum sensing design. Originally from economics, indices such as Gini [6], Pietra-Ricci [7], Atkinson [8], and Theil [9] offer a novel perspective by capturing statistical asymmetries in the received signal. However, their performance has been evaluated, in these works, only under the conventional receiver model. This study extends the analysis by assessing and comparing the performance of inequality-based detectors in centralized CSS with data fusion under both conventional and DCR-based receiver models.

The remainder of this paper is organized as follows: Section II presents the system model, while Section III describes the test statistics adopted for performance evaluation, which is carried out in Section IV. Finally, Section V summarizes the main conclusions drawn from this study.

II. System Model

A. Conventional Receiver Model

This work adopts a centralized CSS model with data fusion, where m SUs collaboratively perform spectrum sensing. Each SU collects n samples of the PU signal during a sensing interval and forwards them to a FC via error-free control channels. The received samples at the FC are arranged in the matrix $\mathbf{Y} \in \mathbb{C}^{m\times n}$, modeled as

$$\mathbf{Y} = \mathbf{h}\mathbf{x}^{\mathrm{T}} + \mathbf{V}, \tag{1}$$

where $\mathbf{x} \in \mathbb{C}^{n\times 1}$ contains the PU signal samples, modeled as zero-mean complex Gaussian random variables with variance defined by the average signal-to-noise ratio (SNR) across the SUs. This statistical model captures envelope fluctuations commonly observed in modulated and filtered signals.

The channel vector $\mathbf{h} \in \mathbb{C}^{m\times 1}$ consists of elements h_i representing the fading coefficients between the PU and the i-th SU. These gains vary over time due to SU mobility and multipath propagation. The channel vector is expressed as

$$\mathbf{h} = \mathbf{G}\mathbf{a}, \tag{2}$$

where $\mathbf{a} \in \mathbb{C}^{m\times 1}$ is composed of complex Gaussian random variables $a_i \sim \mathbb{C}\mathcal{N}[\sqrt{\kappa/(2\kappa+2)}, 1/(\kappa+1)]$. The Rice factor κ is expressed in decibels as $\kappa_{\mathrm{dB}} = 10\log_{10}(\kappa)$ and is modeled as $\kappa_{\mathrm{dB}} \sim \mathcal{N}[\mu_\kappa, \sigma_\kappa]$, where μ_κ and σ_κ, both in dB, characterize the propagation environment [10].

To model heterogeneous and time-varying signal power reception due to SU displacement and different distances to the PU, the matrix $\mathbf{G} \in \mathbb{R}^{m\times m}$ is defined as

$$\mathbf{G} = \mathrm{diag}\left(\sqrt{\frac{\mathbf{p}}{P_{\mathrm{tx}}}}\right), \tag{3}$$

where $\mathbf{p} = [P_{\mathrm{rx}_1}, \ldots, P_{\mathrm{rx}_m}]^{\mathrm{T}}$ contains the received power values at each SU, and P_{tx} is the PU's transmit power, in watts. The received power at the i-th SU is estimated using the log-distance path loss model [11]

$$P_{\mathrm{rx}_i} = P_{\mathrm{tx}}\left(\frac{d_0}{d_i}\right)^{\eta}, \tag{4}$$

where d_0 is a far-field reference distance, d_i is the distance from the PU to the i-th SU, and η is the path loss exponent. All distances are in meters.

Variations in noise power across SU receivers are modeled by the matrix $\mathbf{V} \in \mathbb{C}^{m\times n}$, whose i-th row has zero-mean complex Gaussian entries with variance given by

$$\sigma_i^2 = (1 + \rho u_i)\bar{\sigma}^2, \tag{5}$$

where u_i is a realization of a uniform random variable $U_i \sim \mathcal{U}[-1, 1]$, $\bar{\sigma}^2$ denotes the average noise power, and $0 \le \rho < 1$ controls the variability around the mean.

Given the randomness in both σ_i^2 and d_i, the instantaneous SNR observed at the SUs is itself a random variable, expressed as

$$\gamma = \frac{1}{m}\sum_{i=1}^{m}\frac{P_{\mathrm{tx}}\,(d_0/d_i)^{\eta}}{(1+\rho u_i)\bar{\sigma}^2}. \tag{6}$$

The average SNR across all SUs is defined as $\mathrm{SNR} = \mathbb{E}[\gamma]$, the expected value of γ. As derived in [12], the closed-form expression for this average SNR is

$$\mathrm{SNR} = \frac{\ln\left(\frac{1+\rho}{1-\rho}\right)}{2\rho m\bar{\sigma}^2}\sum_{i=1}^{m} P_{\mathrm{rx}_i}. \tag{7}$$

B. Direct-Conversion Receiver Model

The CSS framework discussed in [5] is built upon a realistic representation of a direct-conversion receiver (DCR), which reflects the signal processing chain typically employed in practical radio front-ends. Although the internal circuitry of the DCR is not detailed here, its operational principles define the model shown in Fig. 1, which serves as the simulation platform for centralized CSS schemes with data fusion. The model explicitly accounts for essential baseband processing steps carried out at the SUs and at the FC, including signal filtering, residual DC-offset injection, automatic gain control (AGC), noise whitening, analog-to-digital conversion (ADC), computation of test statistic, and binary spectrum occupancy decision.

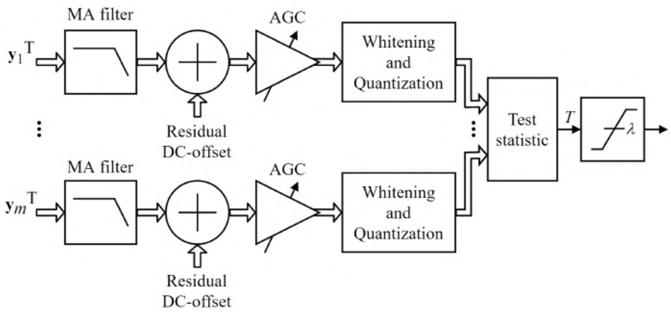

Fig. 1. Simulation model for DCR-based CSS with centralized data fusion [5].

Each row $\mathbf{y}_i^{\mathrm{T}}$ of the received signal matrix $\mathbf{Y}$, comprising the samples collected by the i-th SU, with $i = 1, \ldots, m$, is passed through a moving-average (MA) filter of length L. This filtering stage approximates the cumulative impact of transmitter, channel, and receiver filtering.

Then, the signal is impaired by residual DC-offset components, which emulate the incomplete cancellation of unwanted DC levels that often result from local oscillator self-mixing and strong in-band interferers [4]. These residual offsets are modeled as additive zero-mean Gaussian noise with variance σ_{dc}^2. The severity of this impairment is quantified through the signal-to-DC-offset ratio (SDCR), defined in dB as

$$\mathrm{SDCR} = 10\log_{10}\left(\frac{p_{\mathrm{avg}}}{\sigma_{\mathrm{dc}}^2}\right), \tag{8}$$

where p_{avg} denotes the average signal power prior to DC contamination, given by $\frac{1}{m}\sum_{i=1}^{m} P_{\mathrm{rx}_i}$.

To normalize signal amplitudes across different SUs, an AGC mechanism is applied. The gain applied at the i-th SU is given by

$$g_i = \frac{f_{\mathrm{od}}\sqrt{2n}}{6\|\mathbf{y}_i\|}, \tag{9}$$

where $\|\cdot\|$ is the Euclidean norm, and f_{od} characterizes the variability in clipping levels found in practical ADCs.

Once AGC is applied, the signal is digitized and subjected to a noise whitening [13], which serves to decorrelate the samples affected by the earlier MA filtering. Given its sensitivity to quantization, whitening is performed using high-resolution samples. After whitening, the data is re-quantized at a lower resolution for transmission over a control channel to the FC, thereby reducing the required bandwidth.

In the "Whitening and Quantization" block of Fig. 1, the whitening operation is mathematically represented by a matrix $\mathbf{B} \in \mathbb{R}^{n\times n}$, applied to the AGC-adjusted and quantized signal matrix. The whitening matrix is defined as

$$\mathbf{B} = \mathbf{U}\mathbf{L}^{-1}, \tag{10}$$

where $\mathbf{U}$ is an orthogonal matrix derived from the singular value decomposition of the autocorrelation matrix $\mathbf{Q} \in \mathbb{R}^{n\times n}$, and $\mathbf{L}$ is the Cholesky factor of $\mathbf{Q}$.

The entries of $\mathbf{Q}$ are computed based on the autocorrelation function of the MA filter's impulse response, as follows

$$Q_{ij} = q_{|i-j|}, \tag{11}$$

for $i, j = 1, \dots, n$, with

$$q_k = \begin{cases} 1 - \dfrac{k}{L}, & \text{if } k \leq L, \\ 0, & \text{otherwise}, \end{cases} \qquad k = 0, 1, \dots, n-1.$$

To ensure unit average power after filtering, the MA filter coefficients are normalized as $z_l = 1/\sqrt{L}$ for $l = 1, \dots, L$.

III. Test Statistics

The sample covariance matrix (SCM) estimates the covariance structure of the received signal using a finite number of samples. It captures linear dependencies among signal components and, in the spectrum sensing scenario, is computed at the FC as

$$\hat{\mathbf{R}} = \frac{1}{n}\mathbf{Y}\mathbf{Y}^{\dagger}, \tag{12}$$

where $\dagger$ denotes the Hermitian operator.

The test statistics for the Gini index detector (GID) [6] and the Pietra-Ricci index detector (PRIDe) [7] are defined, respectively, as

$$T_{\text{GID}} = \frac{\sum_{i=1}^{m^2} |r_i|}{\sum_{i=1}^{m^2}\sum_{j=1}^{m^2} |r_i - r_j|}, \tag{13}$$

$$T_{\text{PRIDe}} = \frac{\sum_{i=1}^{m^2} |r_i|}{\sum_{i=1}^{m^2} |r_i - \bar{r}|}, \tag{14}$$

where r_i is the i-th entry of the vector $\mathbf{r}$ formed by column-wise stacking of $\hat{\mathbf{R}}$, and

$$\bar{r} = \frac{1}{m^2}\sum_{i=1}^{m^2} r_i \tag{15}$$

is the empirical mean of the SCM entries.

The Atkinson index detector (AID) [8] test statistic is defined as

$$T_{\text{AID}} = \frac{1}{\bar{r}}\left(\sum_{i=1}^{m}\sum_{j=1}^{m} r_{ij}^{1-\epsilon}\right)^{\frac{1}{1-\epsilon}}, \quad \epsilon \in (0,1) \cup (1,\infty). \tag{16}$$

For the specific case $\epsilon = 0.5$, the expression simplifies to

$$T_{\text{AID}} = \frac{1}{\bar{r}}\left(\sum_{i=1}^{m}\sum_{j=i}^{m}(2-I)\sqrt{|r_{ij}| + \Re(r_{ij})}\right)^2, \tag{17}$$

where $I = 1$ if $i = j$ and $I = 0$ otherwise, enabling computational savings by exploiting the Hermitian symmetry of $\hat{\mathbf{R}}$. The operator $\Re(\cdot)$ retrieves the real part of its argument.

The Theil index detector (TID) [9] uses an entropy-based formulation to quantify inequality among SCM entries. Its test statistic is

$$T_{\text{TID}} = \left[\sum_{i=1}^{m}\sum_{j=i}^{m}(2-I)\,|r_{ij}|\log\left(\frac{|r_{ij}|}{\bar{r}_{\text{abs}}}\right)\right]^{-1}, \tag{18}$$

where

$$\bar{r}_{\text{abs}} = \sum_{i=1}^{m}\sum_{j=1}^{m} |r_{ij}| \tag{19}$$

is the total absolute sum of the SCM entries, and I follows the same definition as in (17).

IV. Numerical Results

In this section, we present computer simulation results for centralized CSS with data fusion, considering both the conventional and DCR models. The evaluation is based on the probability of detection, P_{d}, as a function of various system parameters, assuming a fixed probability of false alarm $P_{\text{fa}} = 0.1$ [14]. Results are provided for the GID, PRIDe, AID, and TID detectors. Each point on the performance curves was obtained from 10000 Monte Carlo runs, using MATLAB R2024b. The simulation code used to generate the results is publicly available in [15].

Using the conventional model under AWGN as a performance baseline, the average SNR or the number of samples collected per SU for each sensing interval, n, were adjusted in some scenarios so that the best-performing detector achieves $P_{\text{d}} \approx 0.9$ at the midpoint of the parameter range under study. This normalization facilitates a clearer comparison of performance trends across different configurations.

Unless otherwise stated, the system parameters are fixed as follows: $m = 6$ SUs, representing a small number of cooperating cognitive radios, which ensures efficient use of the control channel; $n = 250$ samples per SU, chosen to satisfy the desired detection performance; SNR $= -10$ dB, reflecting operation in a low-SNR regime; noise power variation factor $\rho = 0.5$, modeling thermal noise fluctuations; path-loss exponent $\eta = 2.5$, characteristic of urban environments; normalized coverage radius $r = 1$ m; reference distance $d_0 = 0.001r$ for path-loss computation; transmit power $P_{\text{tx}} = 5$ W, chosen to reflect practical PU power levels; and a random Rice factor with mean $\mu_\kappa = 1.88$ dB and standard deviation $\sigma_\kappa = 4.13$ dB, following urban channel measurements from [10].

Fig. 2 illustrates the variation of P_{d} as the SNR increases from -20 to 0 dB. As expected, performance improves with higher SNR values, following a same pattern for all detectors, in both the conventional (left) and DCR (right) scenarios.

Under the conventional model, TID shows the weakest performance at low SNRs but eventually outperforms GID and approaches AID for SNR ≥ -10 dB, while PRIDe becomes the most effective at higher SNRs. Under the DCR model, most detectors maintain similar trends with slight degradation; however, TID experiences a significant performance drop due to its reliance on logarithmic ratios between SCM entries and their mean to measure inequality. Signal processing impairments introduced by the DCR, such as clipping, quantization, and DC-offset, reduce the variability of the SCM, diminishing the discriminative power of the logarithmic function. Consequently, TID becomes less capable of distinguishing between hypotheses $\mathcal{H}_0$ and $\mathcal{H}_1$. In contrast, GID, which relies on absolute differences, PRIDe, which measures deviations from the mean, and AID, which applies square roots that mitigate distortions, exhibit greater robustness to the DCR-induced effects.

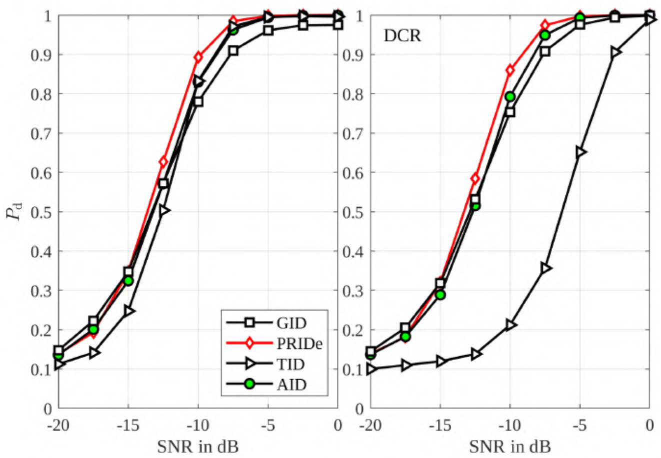

Fig. 2. Probability of detection, P_d, versus signal-to-noise ratio (SNR) in dB under conventional (left-hand side) and DCR (right-hand side) models.

Fig. 3 shows the impact of the path-loss exponent η on detection performance. Although the average SNR across users is kept constant for all values of η by adjusting the noise power accordingly, the effective SNR distribution becomes increasingly unbalanced as η increases, due to growing disparities in the received signal powers at individual SUs arising from their varying distances to the PU transmitter. As propagation conditions worsen, this imbalance reduces the efficiency of cooperative detection. While GID, PRIDe, and AID exhibit relatively robust behavior across the entire η range in both models, TID suffers a significant degradation, especially under the DCR model. This is due to its reliance on logarithmic ratios to measure inequality, which become less discriminative when the SCM entries show reduced variability, a condition exacerbated by DCR-induced impairments such as clipping, quantization, and DC-offset.

Fig. 4 illustrates the impact of the mean of Rice factor, μ_κ, on detection performance. It can be observed that μ_κ begins to significantly influence P_d around -5 dB, which corresponds to the point where the dominant line-of-sight component of the received signal starts to prevail over the scattered components. This leads to performance improvements across most detectors, although with varying intensities. Under the conventional model (left), all detectors benefit from the increase in μ_κ, with GID, PRIDe and AID showing the most pronounced gains. Under the DCR model (right), similar trends are observed for GID, PRIDe, and AID, albeit with slightly reduced performance levels. The TID, however, exhibits pronounced sensitivity to signal distortions, which obscures the statistical structure of SCM, even as channel conditions improve. Consequently, its performance remains nearly constant and notably poor across different values of μ_κ, indicating a lack of adaptability to variations in the Rice factor.

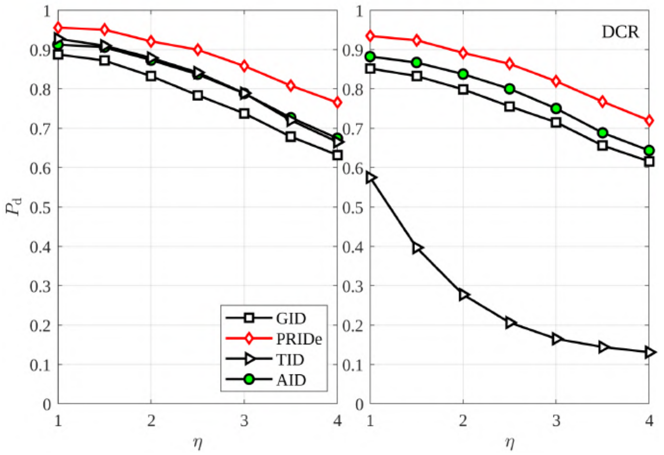

Fig. 3. Probability of detection, P_d, versus path loss exponent, η, under conventional (left-hand side) and DCR (right-hand side) models.

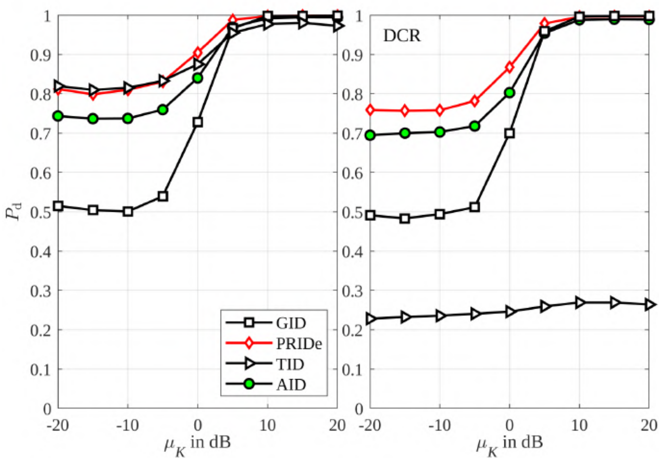

Fig. 4. Probability of detection, P_d, versus mean of Rice factor, μ_κ, for SNR $= -9$ dB under conventional (left-hand side) and DCR (right-hand side) models.

Fig. 5 illustrates the impact of two essential terms of the DCR model. Figs. 5a and 5b show, respectively, the probability of detection, P_d, as a function of the overdrive factor f_od and the SDCR. These two parameters were selected for analysis due to their pronounced influence on detector performance, as observed in preliminary evaluations.

Fig. 5a shows the behavior of P_d versus the overdrive factor, f_od, which controls the input signal amplitude relative to the

ADC dynamic range. All detectors exhibit a mild concave response, indicating a trade-off region. For small values of f_{od}, the input signal occupies only a limited portion of the quantizer's range, resulting in reduced resolution and performance degradation due to insufficient quantization granularity. As f_{od} increases, performance improves until a saturation point is reached, beyond which signal clipping begins to dominate, again impairing detection. Unlike the other detectors, the TID fails to respond to variations in f_{od}, consistently performing poorly. This underscores its vulnerability to quantization and unsuitability for realistic ADC conditions.

Fig. 5b presents the variation of P_{d} versus the SDCR under the DCR model. As expected, low SDCR values, corresponding to stronger residual DC-offsets relative to the received signal, result in poor detection performance across all detectors. As SDCR increases, P_{d} improves steadily up to approximately -5 dB, beyond which performance tends to stabilize. This plateau suggests that for SDCR values above -5 dB, the residual DC-offset becomes sufficiently small so as not to significantly interfere with the detection process. Among the detectors, PRIDe consistently achieves the highest P_{d}, followed by AID and GID, which are similarly affected by the offset. The TID again shows limited adaptability, further confirming its susceptibility to DCR-induced distortions and its reduced ability to exploit the underlying covariance structure when corrupted by practical impairments.

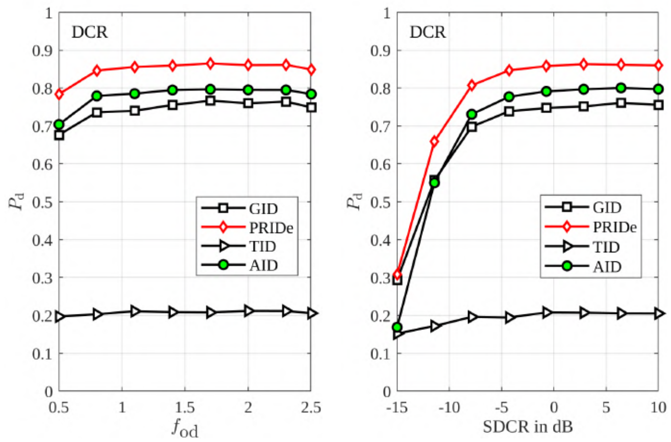

(a) (b)

Fig. 5. Probability of detection, P_{d}, versus specific parameters of the DCR model: overdrive factor f_{od} (5a) and signal-to-DC-offset ratio (SDCR) (5b).

V. Conclusions

This study evaluated the performance of centralized CSS with data fusion under both conventional and DCR receiver models, focusing on the impact of signal processing impairments and system parameters on inequality-based detectors, namely GID, PRIDe, AID, and TID. The analysis considered a fixed P_{fa} scenarios with varying SNR, path-loss exponent η, mean Rice factor μ_{κ}, and DCR-specific parameters such as overdrive factor f_{od} and SDCR. While all detectors benefit from increased SNR and favorable propagation, TID exhibited a marked performance drop under DCR conditions due to its reliance on logarithmic ratios, which are highly affected by quantization, clipping, and DC-offset effects.

In contrast, GID, PRIDe, and AID demonstrated greater robustness, maintaining consistent performance despite receiver impairments. The configuration of DCR-related parameters, particularly f_{od} and SDCR, also proved critical, with improper tuning leading to significant degradation. Among the evaluated schemes, PRIDe stood out as the most resilient detector, followed closely by AID and GID, while TID was confirmed as the most sensitive to realistic distortions. These results underscore the importance of incorporating receiver-aware modeling and accounting for hardware-induced impairments in the design and evaluation of spectrum sensing systems.

References

[1] A. Nasser, H. Al Haj Hassan, J. Abou Chaaya, A. Mansour, and K.-C. Yao, "Spectrum sensing for cognitive radio: Recent advances and future challenge," *Sensors*, vol. 21, no. 7, 2021. [Online]. Available: https://www.mdpi.com/1424-8220/21/7/2408

[2] Y. Arjoune and N. Kaabouch, "A comprehensive survey on spectrum sensing in cognitive radio networks: Recent advances, new challenges, and future research directions," *Sensors*, vol. 19, no. 1, 2019. [Online]. Available: https://www.mdpi.com/1424-8220/19/1/126

[3] D. A. Guimarães, "Spectrum sensing: A tutorial," *Journal of Communication and Information Systems*, vol. 37, no. 1, pp. 10–29, Feb. 2022. [Online]. Available: https://jcis.sbrt.org.br/jcis/article/view/811

[4] D. A. Guimaraes and R. A. A. de Souza, "Implementation-oriented model for centralized data-fusion cooperative spectrum sensing," *IEEE Communications Letters*, vol. 16, no. 11, pp. 1804–1807, 2012.

[5] D. A. Guimarães and E. J. T. Pereira, "Influence of a direct-conversion receiver model on the performance of detectors for spectrum sensing," *Journal of Communication and Information Systems*, vol. 36, no. 1, p. 173–183, Nov. 2021, doi: 10.14209/jcis.2021.19.

[6] D. A. Guimarães, "Gini index inspired robust detector for spectrum sensing over ricean channels," *Electronics Letters*, Nov. 2018, doi: 10.1049/el.2018.7375.

[7] ——, "Pietra-Ricci index detector for centralized data fusion cooperative spectrum sensing," *IEEE Transactions on Vehicular Technology*, vol. 69, no. 10, pp. 12 354–12 358, 2020, doi: 10.1109/TVT.2020.3009440.

[8] ——, "Atkinson index detector for spectrum sensing," *Journal of Communication and Information Systems*, vol. 39, no. 1, p. 189–193, Nov. 2024. [Online]. Available: https://jcis.sbrt.org.br/jcis/article/view/898

[9] D. A. Guimarães, "Detector baseado no índice de theil para sensoriamento espectral cooperativo," in *XLII Simpósio Brasileiro de Telecomunicações e Processamento de Sinais (SBrT)*, Belém, PA, Brasil, Oct. 2024.

[10] S. Zhu, T. S. Ghazaany, S. M. R. Jones, R. A. Abd-Alhameed, J. M. Noras, T. Van Buren, J. Wilson, T. Suggett, and S. Marker, "Probability distribution of Rician K-factor in urban, suburban and rural areas using real-world captured data," *IEEE Trans. Antennas Propag.*, vol. 62, no. 7, pp. 3835–3839, Jul 2014, doi: 10.1109/TAP.2014.2318072.

[11] T. S. Rappaport, *Wireless Communications: Principles And Practice*, 2nd ed. Pearson Education, 2010.

[12] D. A. Guimarães, "Modified Gini index detector for cooperative spectrum sensing over line-of-sight channels," *Sensors*, vol. 23, no. 12, 2023. [Online]. Available: https://www.mdpi.com/1424-8220/23/12/5403

[13] R. Wang and M. Tao, "Blind spectrum sensing by information theoretic criteria for cognitive radios," *IEEE Transactions on Vehicular Technology*, vol. 59, no. 8, pp. 3806–3817, 2010.

[14] The Institute of Electrical and Electronics Engineers (IEEE), "IEEE 802 Part 22: Cognitive Wireless RAN Medium Access Control (MAC) and Physical Layer (PHY) Specifications: Policies and Procedures for Operation in the TV Bands," IEEE, Standard IEEE Std 802.22-2011, 2011, accessed: 2025-04.

[15] D. A. Guimarães and L. G. B. Guedes, "Influence_of_dcr_on_performance_of_detectors_v1.m," https://github.com/luizgustavobguedes/Spectrum-Sensing/blob/main/Influence_of_DCR_on_Performance_of_Detectors_v1.m, 2024, Accessed: 2024-04-20.